HHS Public Access

Author manuscript

J Control Release. Author manuscript; available in PMC 2018 March 10.

Published in final edited form as:

J Control Release. 2017 March 10; 249: 173–182. doi:10.1016/j.jconrel.2017.01.032.

Generation-6 hydroxyl PAMAM dendrimers improve CNS penetration from intravenous administration in a large animal brain injury model

Fan Zhang[a,f,1], **J. Trent Magruder**[b], **Yi-An Lin**[a], **Todd C. Crawford**[b], **Joshua C. Grimm**[b], **Christopher M. Sciortino**[b], **Mary Ann Wilson**[c,d], **Mary E. Blue**[c,d], **Sujatha Kannan**[c,e], **Michael V. Johnston**[c,d], **William A. Baumgartner**[b,*], and **Rangaramanujam M. Kannan**[a,*]

[a] Center for Nanomedicine/Wilmer Eye Institute, Department of Ophthalmology, The Johns Hopkins School of Medicine, Baltimore, Maryland 21287, United States

[b] Division of Cardiac Surgery, Department of Surgery, The Johns Hopkins University School of Medicine, Baltimore, Maryland 21287, United States

[c] Hugo W. Moser Research Institute at Kennedy Krieger Inc., Baltimore, MD 21205

[d] Department of Neurology, The Johns Hopkins University School of Medicine, Baltimore, Maryland 21287, United States

[e] Department of Anesthesiology and Critical Care Medicine, The Johns Hopkins University School of Medicine, Baltimore, Maryland 21287, United States

[f] Department of Materials Science and Engineering, The Johns Hopkins University, Baltimore, Maryland, 21218, United States

Abstract

Hypothermic circulatory arrest (HCA) provides neuroprotection during cardiac surgery but entails an ischemic period that can lead to excitotoxicity, neuroinflammation, and subsequent neurologic injury. Hydroxyl polyamidoamine (PAMAM) dendrimers target activated microglia and damaged neurons in the injured brain, and deliver therapeutics in small and large animal models. We investigated the effect of dendrimer size on brain uptake and explored the pharmacokinetics in a clinically-relevant canine model of HCA-induced brain injury. Generation 6 (G6, ~6.7 nm) dendrimers showed extended blood circulation times and increased accumulation in the injured brain compared to generation 4 dendrimers (G4, ~4.3 nm), which were undetectable in the brain by 48 hrs after final administration. High levels of G6 dendrimers were found in cerebrospinal fluid (CSF) of injured animals with a CSF/serum ratio of ~20% at peak, a ratio higher than that of many neurologic pharmacotherapies already in clinical use. brain penetration (measured by drug

[*]**Corresponding Authors:** Rangaramanujam M. Kannan, krangar1@jhmi.edu, Address: 400 N. Broadway / Smith Bldg 6th Floor 115, Baltimore, Maryland 21231, William A. Baumgartner, wbaumgar@jhmi.edu, Address: 733 Broadway St, MRB-Ste, Baltimore, MD 21287.

[1]Present address: Fred Hutchinson Cancer Research Cancer, 1100 Fairview Ave. N., Seattle, WA 98109.

CSF/serum level) of G6 dendrimers correlated with the severity of neuroinflammation observed. G6 dendrimers also showed decreased renal clearance rate, slightly increased liver and spleen uptake compared to G4 dendrimers. These results, in a large animal model, may offer insights into the potential clinical translation of dendrimers.

Graphical abstract

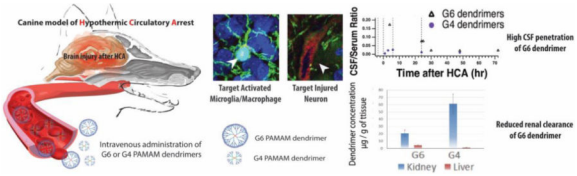

Keywords

Dendrimer; hypothermic circulatory arrest; canine model; brain penetration; CSF/serum ratio; biodistribution

Introduction

Hypothermic circulatory arrest (HCA) provides neuroprotection during complex cardiac surgical operations that require partial or complete interruption of the cerebral circulation. These include certain procedures involving repair or replacement of the aortic arch, as well as congenital heart surgery [1-4]. Despite these advances, HCA continues to be associated with neurological sequelae in both pediatric and adult patients [4, 5]. For over 20 years, Baumgartner and colleagues have utilized a model of HCA in large canine subjects. This technique involves peripheral cannulation for cardiopulmonary bypass (CPB), followed by systemic cooling on CPB to 18 °C, at which point canines are subjected to a 60-120 minutes' period of HCA followed by rewarming and resuscitation (Figure 1). Glutamate-mediated excitotoxicity [6, 7] and neuroinflammation [8] are major pathological mechanisms that lead directly to brain injury in the hippocampus, cortex, basal ganglia and cerebellum in this model [9-12]. Accordingly, to mitigate excitotoxicity and neuroinflammation, therapeutics should be delivered to injured neurons and activated glial cells in injured brain regions [12]. Unfortunately, current therapeutic interventions have not yet shown significant efficacy in improving neurological outcomes. This is due in part to the limited ability of small drug molecules to cross the blood-brain barrier (BBB), resulting in relatively poor accumulation in the central nervous system (CNS) and cerebrospinal fluid (CSF). Free drug therapies also expose patients to the risk of drug toxicity at higher doses [13-15].

We have demonstrated that hydroxyl-terminated generation 4 polyamidoamine (PAMAM) dendrimers (G4 dendrimers) provide site-specific delivery of small molecular drugs across the BBB and blood-CSF barriers, specifically targeting the injured brain in this canine HCA model [12]. However, greater brain accumulation and enhanced CSF penetration could be beneficial for translating dendrimer-based therapies from animal studies to humans, where dose and toxicity concerns are paramount. G4 dendrimers, though able to specifically target

injured brain regions in our canine HCA model, have rapid systemic clearance in many species, including canine [12], rabbit [16], rat [17], and mouse [18]. Such rapid clearance limits dendrimer accumulation in injured brain regions. In this study, we tested the hypothesis that the use of larger size dendrimers would enhance dendrimer accumulation in the brain due to delayed clearance and prolonged systemic circulation while maintaining their intrinsic targeting ability to activated microglia and injured neurons.

Plasma-binding properties and nanoparticle size are the two dominating factors that define *in vivo* clearance rate and secretion pathway. Nanoparticles that have a hydrophobic surface or charged surface properties are more likely to interact and bind with plasma proteins during systemic circulation, and to induce opsonization that leads to elevated reticuloendothelial system (RES) clearance and increased liver uptake [19, 20]. G4 dendrimers, which have a neutral surface charge, have fewer interactions with key human plasma proteins *in vitro* [21], and are generally considered as non-plasma binding nanoparticles. For these nanoparticles, particles size plays the primary role in determining the mode of clearance [22]. The upper limit for effective glomerular filtration lies between 6–8 nm [20]. In general, nanoparticles can be cleared efficiently by renal glomeruli at diameters below this range. Alternatively, nanoparticles larger than this range are less likely to be cleared through renal filtration [23]. These nanodevices, if not dissociable or degradable rapidly, tend to be cleared by the reticuloendothelial system (RES) and are cleared by the liver [20].

Generation 6 (G6) dendrimers with hydroxyl terminal groups have a hydrodynamic diameter around 6.7 nm (~1.5-fold higher than G4 dendrimers) and provide similar surface properties as G4 dendrimers (neutral and hydrophilic). Like the G4 dendrimer, they are unlikely to bind with serum proteins in the plasma. However, the G6 dendrimer's size lies on the edge of the renal filtration range; therefore, this slight increase in size can potentially extend the circulation period after systemic dendrimer administration without altering the major renal clearance pathway.

In this study, we determined the pharmacokinetics of G6 dendrimers in a clinically relevant large animal model, with a focus on 1) how the G6 dendrimer's increased size affects its systemic circulation time and clearance pathway, and 2) whether these changes in biodistribution profiles can enhance the targeting characteristics in the injured brain as compared to the G4 dendrimer (G4 dendrimer data was obtained from our previous experiments in this canine model [12]). The comparison of pharmacokinetics and biodistribution of G6 dendrimers with G4 dendrimers may offer clinical insight and significance in translating dendrimer research into human trials.

Materials and Methods

Synthesis of G6-Cy5

The synthesis (Figure 1A), characterization (Figure S1-4), and purification of G6-Cy5 were based on our previously published work for labeling G4 PAMAM dendrimers [12]. All reagents were purchased from Sigma-Aldrich (St. Louis, MO) unless further noted. In an oven-dried round bottom flask, 6-Fmoc-capronic acid (100 mg, 0.283 mmol), PyBOP (216 mg, 0.415 mmol; Bachem, Torrance, CA), and N,N-Diisopropylethylamine (DIEA) (100 μL,

0.574 mmol) were combined and dissolved in anhydrous Dimethylformamide (DMF) (15 mL) under N_2 gas environment. This reaction mixture was stirred at 0 °C for 15 min. This solution was then combined with generation 6 hydroxyl-terminated PAMAM dendrimer (1.100 g, 0.01887 mmol; Dendritech, Inc., Midland, MI) that was initially dissolved in anhydrous DMF (25 mL). The reaction was continued for 48 hrs at room temperature. The solution was then concentrated *in vacuo* for 20 min to remove DMF and DIEA, with temperature maintained at around 25 °C during this process. To proceed for dialysis, concentrated reaction mixture was redissolved in ~100 mL of DMF and was dialyzed against 2 L of DMF for 24 hrs (Molecular weight cutoff (MWCO): 8 kD), with dialysis solvent replaced every 8-12 hrs. The dialyzed solution was then concentrated under reduced pressure and dried over high vacuum to yield the first intermediate. To proceed with Fmoc deprotection, this crude material was then dissolved in anhydrous DMF (5 mL) and mixed with piperidine/DMF (1:4; 10 mL) in ice bath for 15 min. The reagents were then removed under reduced pressure until dry. The residue was then redissolved in DMF and then dialyzed against DMF (MWCO: 8kD) for 24 hr. The dialyzed solution was then concentrated *in vacuo*, redissolved in DI H_2O, and dialyzed against DI H_2O for 2 hrs. The obtained aqueous solution was then lyophilized to yield the dry mass of bifunctional dendrimer G6-$(OH)_{249}$-$(NH_2)_7$. The bifunctional dendrimer (200 mg) was dissolved in anhydrous DMF (4 mL), which was later mixed with triethylamine (100 μL) and Cy5-mono-NHS ester (10 mg; GE Healthcare, Pittsburgh, PA) that was dissolved in anhydrous DMSO (2 mL). The reaction was carried out overnight and then concentrated under reduced pressure. The residue was redissolved in DMF and dialyzed against DMF (MWCO: 8kD) for 48 hr. The dialyzed solution was concentrated, re-dissolved in H_2O, and then dialyze against H_2O (MWCO: 8 kD) for 2 hrs. The dialyzed solution was then lyophilized to give the dry mass of G6-Cy5 deep blue solids. The final conjugates were characterized by ^{1}H-NMR (Figure S1), RP-HPLC (Figure S2), and fluorospectroscopy (Figure 1B and Figure S3).

Surgical procedure of hypothermic cardiac arrest and dendrimer administration

The canine model of HCA used is as described previously [9]. Class-A 30 kg male hounds, 6-12 months old, were used in this study. Experimental approval was obtained from the Johns Hopkins University Animal Care and Use Committee (D0313M06) and all relevant members of the surgical and care teams underwent appropriate training prior to initiation of the study. The dogs were anesthetized with methohexital sodium (12 mg/kg i.v., in divided doses) and maintained on isoflurane inhalational anesthesia, i.v. fentanyl (150-200 μg/dose), and midazolam (2.5 mg/dose) following endotracheal intubation. Temperature probes were placed in the ear (tympanic membrane), esophagus, and rectum for the duration of the experiment. A left femoral arterial pressure catheter also was placed for continuous monitoring of blood pressure and arterial blood sampling. Continuous electrocardiographic monitoring was employed.

All dogs were given a total dose of 6 mg/kg G6-Cy5; the dendrimers were dissolved in sterile saline, followed with immediate filtration through membrane of 0.4 μm pore size prior to the administration. The G6-Cy5 was administered as three separate doses prior to and post HCA (Figure 1C). Initially, 10% of the total G6-Cy5 dose was administered as an intravenous bolus on the morning of surgery prior to initiation of CPB. Animals were then

heparinized and peripherally cannulated for CPB with one femoral arterial cannula (advanced into the descending thoracic aorta) as well as femoral and external jugular venous cannulae (advanced through the inferior and superior vena cavae, respectively, into the right atrium). The animals were cooled to 18°C, and then underwent 90 minutes of HCA with standard hemodilution and alpha-stat regulation of arterial blood gases. After HCA, CPB was reinstituted, the animal was rewarmed (5°C/15 min) to 37°C, and subsequently 70% of the overall G6-Cy5 dose was infused over a 6 hrs time span. The CPB cannulae were then removed, hemostasis achieved, and heparinization was reversed with protamine (3 mg/kg). After canines were hemodynamically and clinically stable, the animals were transferred to a cage for recovery and provided with analgesia as needed. An additional bolus dose (20% of total dose) was given at 24 hrs after the HCA procedure (i.e., morning of postoperative day 1). At 72 hrs after HCA (48 hrs after the last dendrimer administration), the animals were anesthetized, intubated, and maintained on inhalational agents. A median sternotomy was performed followed by proximal aortic cannulation. Cold saline was then infused via an aortic cannula, and the animals were exsanguinated into the thorax. Major organs (brain, heart, lung, liver, kidney, pancreas, spleen) were collected and snap frozen for biodistribution analysis. To evaluate dendrimer pharmacokinetics, CSF (~100 μL), serum (~500 μL) and urine (5-10mL) were collected at representative time points during the whole experiment. Slow intravenous infusion of normal saline was performed after CSF and blood draw for volume correction.

G6-Cy5 extraction and quantification of G6-Cy5 in biofluids and tissues

Dendrimer extraction and quantification followed previous protocols [12]. For liquid samples (such as serum, urine or CSF), the fluid was directly diluted with DPBS at least 10-fold to fit into the linear detection range of our spectrofluorophotometer (Shimadzu RF5301-PC, Shimadzu Scientific Instrument Inc. USA, Columbia, MD). Fluorescence intensities were converted to G6-Cy5 concentration using calibrated samples of known concentrations of G6-Cy5. For tissue samples, approximately 100 mg of tissue was sliced from each organ and then homogenized by a bullet blender for 10 min. The homogenized tissue then was mixed with 1 mL MeOH per 100 mg of tissue, vortexed, and bath sonicated for 10 min to give a cloudy suspension that later was centrifuged at 15000 rpm (14.4 rpm) for 15 min at 4 °C to separate the tissue precipitates and supernatant. As above, fluorescent intensities were converted to levels of G6-Cy5 using a G6-Cy5 calibration curve in MeOH. All calibration curves exhibited high linearity with $R^2 \sim 0.99$. For dendrimer extraction, the recovery rate was higher than 95%.

Immunofluorescence staining

Slices (1 to 2 mm) of freshly harvested hippocampal tissue were fixed by immersion in 4% neutral buffered formalin for 8 hrs followed by cryoprotection in graded sucrose solutions. Cryostat sections (30 μm) were processed for immunohistochemical detection of microglia/macrophages (rabbit anti-Iba1, Wako Laboratory Chemicals #019-19741, 1:2,000, overnight at 4°C), astrocytes (rabbit anti-GFAP, Dako Z0334, 1:5,000, overnight at 4°C), or neurons (mouse anti-beta III tubulin-Alexa Fluor® 488, Abcam #169556, 1:600, 4 hrs at RT). Rabbit primary antibodies were detected using goat-anti-rabbit-Alexa Fluor® 488 (LifeTechnologies, 1:500, 1 hr at RT). A DAPI (4′,6-Diamidino-2-phenylindole

dihydrochloride) nuclear counterstain was used to delineate neuroanatomic regions. Coverslips were mounted using Dako fluorescence anti-fade mounting media.

Confocal microscopy study of G6 dendrimer distribution in brain, kidney, liver, and spleen

Stained tissue sections were imaged under a confocal LSM 710 microscope (Carl Zeiss; Hertfordshire, UK) and processed by ZEN 2011 software. Imaging settings were optimized for each organ or cell type to observe G6-Cy5 localization within microglia, neurons, and astrocytes in the brain, or for G6-Cy5 distribution in the kidney, liver, and spleen. To compare G4 and G6 dendrimers distribution, all imaging settings including laser index, pinhole size, gain, imaging speed, and image quality were kept consistent across all animals.

Results and Discussion

The prolonged circulation of G6 PAMAM dendrimer in serum

We evaluated the *in vivo* stability of G6-Cy5 by RP-HPLC analysis of serum samples acquired at different time points after G6-Cy5 administration (Figure S4 A-I). A fluorescence detector (λ_{ex} = 645 nm, λ_{em} = 660 nm) and the photodiode array (PDA) was used to detect G6-Cy5 and free Cy5 (Figure S4 A and B) and all collected samples. G6-Cy5 was detected in all serum samples (Figure S4 B, C, D), and the UV spectrum of eluted dendrimers from all serum samples (Figure S4 G, H, I) had the same pattern as standard G6-Cy5 (Figure S4 E, F), though there was a slight delay in retention time (0.6 min delay compared with the standard G6-Cy5 sample) (Figure S4 B). None of the tested serum samples contained free Cy5, as compared with the standard free Cy5 peak. Quantifications of dendrimer levels in biofluids/tissues were based on the fluorescence intensity of G6-Cy5 measured at the emission peak (662 nm) (see Figure 1B for the fluorescence spectra).

In this experiment, we used a dosing regimen that differed from the G4 dendrimer experiment (which was simply a 1 hr i.v. infusion after HCA). The current administration protocol of G6 dendrimers in our canine HCA model was designed to be more clinically relevant and, potentially, to address injury as it occurred. We administered 10% of the total dose as a bolus at 3 hrs prior to the conclusion of HCA and infused 70% of the total dose between 0-6 hrs immediately after HCA (Figure 1C). At 24 hrs after HCA, the remaining 20% of the total dose was injected as a bolus. This regimen allows the G6 dendrimers to pre-circulate in the blood before the HCA-induced injury increases BBB permeability. Therefore, we hoped that already-circulating dendrimers would guarantee rapid dendrimer arrival to foci of injury.

Although the dosing regimens used to deliver G4 and G6 dendrimers differed, both G4 and G6 dendrimer doses were completely administrated by 47 hrs prior to the experiment's conclusion. Therefore, the dendrimer concentration during the last 47 hrs of each experiment should be a reasonable window to compare the systemic circulation of G4 and G6 dendrimers. In general, the G6 dendrimer levels in the serum rose during the dendrimer infusion (0-6 hrs after HCA), peaking at around 6–7 hrs after HCA and then plummeting before the second bolus dose that was given at 24 hrs after HCA (Figure 2A). During the following 6 hrs after the second bolus, G6 dendrimers level in serum hovered around 28–

36% of cumulative dose (dose being administered at the time of evaluation; the calculation was based on a 30 kg dog, and the serum volume was estimated to be ~1400 mL) [24]. The concentration of G6 dendrimers gradually decreased afterwards to ~17.4% of cumulative dose at 72 hrs after HCA among the 4 monitored animals. In our previous study of the canine HCA model, G4 dendrimers were able to remain in the serum at a concentration of 7.04 μg/mL at 47 hrs post infusion, which was 6.5% of total dose [12]. Our results for G6 dendrimers showed that a higher percentage of the ID (17.4%) was present in the serum at a later longer time point (66 hrs after 80% of the total dose was given; 48 hrs after the total dose was given than the G4 dendrimer). This 17.4% represents over twice the percentage of that seen for G4 dendrimers, suggesting that G6 dendrimer circulation time was longer than that for G4 dendrimers in this canine model.

G6 dendrimers show enhanced CSF partition and brain uptake in HCA dogs

To assess the G6 dendrimer's CNS penetration, we measured G6 dendrimer CSF levels at various time points. The G6 dendrimer concentrations in CSF were normalized by their respective concentrations in the serum (Figure 2B). Among the four animals, CSF/serum ratio varied: animals 1 and 2 demonstrated overall higher CSF/serum ratios than animals 3 and 4. After the first bolus dose (10% of total dose) and during the 6 hrs of G6 dendrimer infusion (70% of total dose), the CSF/serum ratio for animals 1 and 2 reached 0.2–0.4. At the end of the experiment (48 hrs after the last dose; hour 75), the CSF/serum ratio for animal 1 and 2 was approximately 0.04. For animals 3 and 4, the CSF/serum ratios were around 0.02–0.002 throughout the whole experiment. To further assess these differences, we measured the accumulation of G6 dendrimers in different brain regions (Figure 2C). At 48 hrs after the last dose of G6-Cy5 (72 hrs after HCA), G6 dendrimer accumulation was highest in the hippocampus followed by cerebellum and then the cortex (mean values were 129 ± 56 ng/g in hippocampus, 116 ± 22 ng/g in cerebellum and 68 ± 16 ng/g in cortex (Figure 2C). G6 dendrimer accumulation in hippocampus, the most injured region, was most closely correlated with the CSF/serum ratio in each animal.

The CSF/serum ratio for G6 dendrimers ranged from 0.02–0.20 (on average) during the entire monitoring period, which is close to several common neuroactive agents *(leptin, morphine, phenobarbital)* after repetitively dosed to patients on daily bases [25, 26, 27]. When evaluating area under the curve (AUC) to determine the profile of CSF/serum ratios over time, the AUC of G6 dendrimers is also higher than several clinically used antibiotics, such as penicillin, cloxacillin, amoxicillin, piperacillin, clavulanatem, and cephalosporins (data not shown) [28]. Most systemically administrated drugs or blood-derived proteins have very limited CSF penetration ability, as the trafficking of molecules from blood to the CSF is restricted by selective permeation at the blood-CSF barrier [28]. In normal physiology, tight junctions between endothelial cells maintain the integrity of the blood-CSF barrier. However, the blood-brain barrier (BBB) is disrupted after HCA [7, 12, 29, 30], which creates an opportunity for nanoparticles to enter the brain parenchyma. Although the precise size of blood-CSF barrier leakage in the HCA-induced brain injury is unclear in this model, our results suggest that crossing of the BBB is facilitated by the hydroxyl-terminated PAMAM dendrimers' sub-10 nm size and neutrally-charged surface properties.

PAMAM dendrimers also have been observed to cross the BBB in other CNS disease models, including ischemia/reperfusion injury [31], ischemia-induced white matter injury [32], cerebral palsy [16], and brain tumors [17, 33]. However, the size chosen could still impact the accumulation level in the CSF and brain parenchyma. In this study, G6 dendrimers have a hydrodynamic diameter of 6.7 ± 0.6 nm, which is small enough to penetrate the disrupted blood-CSF barrier, but also to allow for longer systemic circulation compared to G4 dendrimers (~4.3 nm). Moreover, in the presence of inflammation, CSF outflow may decrease, leading to a reduction of CSF production and absorption rates that also increase the retention of G6 dendrimers in the CSF.

The accumulation of G6 dendrimers in brain tissue at 48 hrs after final bolus dose was much higher than that of G4 dendrimers at both 6 hrs post i.v. infusion (~30 ng/g in hippocampus, ~10 ng/g in cortex, and ~60 ng/g in cerebellum) and 24 hrs post i.v. infusion (undetectable at all 3 brain regions, detection limit ~10 ng) (Figure 2C). In addition, the decreased duration of HCA (1.5 hrs, as compared to 2.0 hrs for the G4 dendrimer study) in the present study would be expected to cause less BBB impairment and decreased dendrimer brain penetration. Nonetheless, we observed a higher brain accumulation ratio for G6 versus G4 dendrimers. Although other differences existed between the two studies in terms of injection dose, severity of brain injury, and dosing regimen (Table 1), G6 dendrimers showed 10-fold higher brain accumulation 48 hrs after injection of the last dose compared to G4 dendrimers 47 hrs after 1 hr i.v. infusion. These data indicate that G6 dendrimers have enhanced brain uptake compared to G4 dendrimers. In consideration of the experimental ethics and expenses involved in large animal studies, we made a small modification of the protocol (the HCA time, and dosing regimen) in the G6 dendrimers experiment (Table 1). However, the results from two experiments are still comparable at selected time points. The comparison of pharmacokinetics and biodistribution of G6 dendrimers with G4 dendrimers may offer significant insights into their payload delivery differences, which may be critical in clinical translation.

G6 dendrimer's CNS penetration is associated with the severity of CNS inflammation

Although all HCA animals in this study demonstrated enhanced CSF penetration and brain uptake, the extent of CSF partition and brain uptake varied among animals. Recent review pointed out the connections between hallmarks of CNS inflammation (BBB impairment, microglia/macrophage activation) and nanoparticles uptake by the CNS cells [34]. Here, we compared the extent of neuroinflammation among these animals by measuring interleukin 6 (IL-6) and interleukin 8 (IL-8) levels in the CSF at different time points. IL-6 and IL-8 concentrations in the CSF peaked 4–8 hrs after HCA (Figure 3), during the period when G6 dendrimers were infused intravenously and serum G6-Cy5 levels were maximal. The peak concentrations of IL-6 and IL-8 varied among the 4 animals, indicating that CNS inflammation varied after the 90-min HCA procedure. Interestingly, we found the peak concentrations of IL-6 and IL-8 among the 4 HCA animals followed the same trend (Animal 1>Animal 2>Animal 3>Animal 4) as their respective dendrimer CSF/serum ratios and dendrimer hippocampal accumulations. There was a strong correlation between the peak CSF concentration of IL-6 (R^2=0.91) and IL-8 (R^2=0.95) and the dendrimer CSF/serum ratio after all G6 dendrimers were administered (24 hrs after HCA) among the 4 animals

(Figure S5). Although our sample size was limited in this study, this trend suggests that the ability of G6 dendrimers to cross the BBB correlated directly with the extent of CNS inflammation.

G6 dendrimers selectively accumulate in the injured hippocampus

The hippocampus is the most severely injured brain region in this HCA model [9]. Glutamate-induced excitotoxicity causes cell death in the hippocampus [35], while ischemia-reperfusion injury contributes to early microglial activation in the hippocampus [36]. Our prior histological analyses of the hippocampus demonstrated that neuronal death occurred primarily by apoptosis in the dentate gyrus and by necrosis in the CA region [37]. Of the three major regions of the hippocampus (dentate gyrus, CA1, and CA3) examined by confocal microscopy in this study, the dentate gyrus showed the greatest uptake of G6 dendrimer, followed by CA1 and CA3 regions (Figure 4A–D). In the dentate gyrus, G6 dendrimers were scattered in deeper regions of the granule cell layer where more injured neurons are found (Figure 4D). In the CA1 and CA3 regions, G6 dendrimers accumulated within necrotic neurons and within the walls of blood vessels in presumed endothelial cells (Figure 4B–C).

G6 dendrimer uptake is associated with cell types in hippocampal sub-regions

Since the G6 dendrimer distribution showed different patterns of uptake in the dentate gyrus, CA1, and CA3, we used immunohistochemistry to classify the cell types taking up dendrimer. We used antibodies directed against Iba1 to identify microglia (Figure 5A), TUJ1 to identify neurons (Figure 5B), and GFAP to identify astrocytes (Figure S6). G6 dendrimers were localized in many microglial cells in the dentate gyrus; they were found within the microglial cell bodies and processes, as clustered foci (Figure 5A).

Neurons exhibited less frequent G6 dendrimer uptake and a more diffuse distribution pattern within the soma and larger dendrites than microglia (Figure 5B). To better show the G6 dendrimer's neuronal co-localization, we used a higher gain to process neuronal images. In the CA1 region, G6 dendrimers were internalized only in necrotic pyramidal neurons that have smaller and deformed cell bodies (Figure 5B, magnified images 1 and 2), but not in healthy neurons that have larger, rounded cell bodies (Figure 5B, magnified image 3). We did not observe obvious co-localization of G6 dendrimers in astrocytes (Figure S6).

Differences between microglia and neurons in terms of G6 dendrimer uptake quantity and intracellular distribution may be associated with different uptake mechanisms [38, 39]. In the presence of inflammation, the activated microglia/macrophages in the CNS take up nanoparticles that cross the BBB; this uptake is associated with increased phagocytosis by activated microglia/macrophages (i.e., receptor-mediated endocytosis) [40-42]. On the other hand, internalization of nanoparticles by neurons only has been reported in few studies [43, 44]. Although *in vitro* study on hippocampal neuron showed clathrin mediated pathway as a main internalization pathway for G4 PAMAM dendrimers with amine terminal function groups [45], *in vivo* study of dendrimer uptake by neurons under pathological condition was rarely reported. In our model, hippocampal neurons receive a major glutamatergic input to hippocampus from the neurons in the entorhinal cortex (perforant pathway) [6, 35] and

during ischemia-reperfusion are likely to exhibit abnormally high firing rates. Under such pathologic conditions, G6 dendrimers in the brain parenchyma could be taken up as part of this process. Our observation that G6 dendrimers only localize within injured neurons, but not in adjacent healthy neurons is consistent with our hypotheses about the mechanisms of G6 dendrimer update, but further studies are needed to fully characterize them.

G6 Dendrimers showed reduced renal clearance and increased hepatic clearance

The total quantity of dendrimers in major organs were estimated by multiplying organ weights by the dendrimer concentrations determined in the extracts from the organs (Figure 6A, B). In the kidney, G6 dendrimers were mostly localized in the cortex (20.6 μg/g), rather than in the medulla (3.6 μg/g), and accounted for approximately 1% of the total dose. Confocal microscopy indicated that G6 dendrimers were filtered by glomeruli and accumulated in the proximal tubules, where reabsorption occurred (Figure 6C). The liver and spleen had similar G6 dendrimer concentrations (data not shown), and after considering organ weight, the liver and spleen took up 1.5% and 0.5% of total dose, respectively (Figure 6A). The dendrimer distribution in the liver and spleen was further investigated by confocal microscopy. In liver, G6 dendrimers appeared in sinusoids and downstream in the central vein. In spleen, G6 dendrimers mostly were localized in the red pulps and the marginal zone around the white pulps: they did not penetrate into the white pulps. These observations indicate that the reticuloendothelial system (RES) might play a major role in hepatic and splenic dendrimer accumulation (Figure 6C). In total, about 3.3 ± 0.6% total dose remained in all major organs when the animal was sacrificed (72 hrs after HCA). The liver and the kidney accounted for most of the G6 dendrimer accumulation in major organs (~1.5% and ~1% of overall ID, respectively), followed by spleen, lung, heart, and pancreas (Figure S7). At 72 hrs after HCA, we estimated that 80% of G6-Cy5 ID was cleared.

The distribution of G6 dendrimers differed from that of G4 dendrimers. According to our previous study in the canine model, G4 dendrimer concentration in the kidney was 26.3-fold and 54.6-fold higher than its concentration in the liver after 6 hr or 48 hr post i.v. injection, respectively. G4 dendrimers (~ 4.3 nm) were removed mainly through renal clearance and retained more in the kidney cortex after 48 hrs. In contrast, the concentration of G6 dendrimers in the kidney was only 4.5-fold higher than that in the liver under the current protocol (Figure 6B). This was also reflected in the fluorescence-based imaging of kidney tissue slices, where G4 dendrimers showed much higher intensity in the kidney tubules than G6 dendrimers (Figure 6C). Still, G6 dendrimers were partially excreted into urine, as evidenced by a rapid increase in urine dendrimer levels concordant with the administration time of dendrimers (peaked when infusion was finished and after second bolus dose; see Figure S8). In this case, the ratio of AUC in urine to that in serum indicates the efficiency of renal clearance between the G6 and G4 dendrimers. During the first 5 hrs after the final bolus dose, this ratio was 3.69 for G4 dendrimers, while G6 dendrimers exhibited a much lower value (0.67). Moreover, the ratio was 3.77 and 0.57 for G4 dendrimers and G6 dendrimers during the entire monitored period respectively (Table 1). The decrease in ratios of AUC_{urine} to AUC_{serum} suggests a reduced renal clearance rate for G6 as compared to G4 dendrimers. We also observed a four-fold increase in the G6 dendrimer's concentration in the liver compared to G4 dendrimer at 48 hrs post the last dose (Figure 6B and Table 2), and

enhanced liver and spleen uptake for G6 dendrimers (Figure 6C), indicating the decreased renal clearance rate was associated with increased RES system G6 dendrimer uptake. These results demonstrated that the increase in dendrimer size (4.3 nm to 6.7 nm) significantly impacted the rate of renal clearance, when dendrimer surface properties remain unchanged.

Generally, the renal filtration threshold is considered to be 6-8 nm [20]. For nanoparticles of this intermediate size, surface functionality plays a key role in determining elimination mechanisms [19]. In many instances, nanoparticles that do not interact with serum proteins (normally neutrally or negatively charged) tend to be removed through renal clearance if they are smaller than 6 nm, whilst nanoparticles larger than this size would generally be cleared through liver. This size-cutoff effect has been observed for dendrimers or inorganic nanomaterials such as gold nanoparticles, silica nanoparticles, quantum dots, or iron oxide nanoparticles [46-50]. Reportedly, nanoparticles ~6 nm in size, categorized as the intermediate size within the transition range, could provide different pharmacokinetic outcomes. For instance, in a murine model, hydroxyl-terminated PAMAM dendrimers have been shown to exhibit relatively increased hepatic compared to renal accumulation when the generation increases from G5 (~4.6 nm) to G6 (~6.0 nm). This suggests hepatic clearance of nanoparticles at this size plays an important role [46]. This observation was also noted in another study, which found that 4.3 nm PEG_{350} functionalized Au nanoclusters, ^{64}Cu-alloy were mainly cleared through both kidney filtration and the hepatic excretion routes [51]. However, other studies have reported conflicting results. One found that a 6.7 nm negatively charged gold nanoparticle was predominantly cleared in the kidney (~70% ID and <5% ID underwent renal and feces excretion, respectively, after 72 hr) [49]. Another biodistribution study in a mouse model found that 7-nm RGD-PEG functionalized silica nanoparticles were removed mainly through renal clearance (~72% ID excretion after 96 hr) rather than RES clearance (~15% ID excretion after 96 hr) [48]. Our results imply both renal/hepatic systems may participate in dendrimer clearance for the HCA canines, since G6 dendrimers mainly accumulates in the kidney and liver. These results reflect the representative pharmacokinetics of nanomedicine in similar large animal models. We believe that, taken together, our biodistribution results in a clinically relevant large animal model of a commonly used surgical technique will be highly relevant to the performance of PAMAM dendrimers in clinical trials.

Conclusions

In this study, we demonstrated that G6 PAMAM dendrimers with a hydroxyl group-functionalized surface are better vehicles for targeting injured CNS cells in a 30 kg canine brain injury model than G4 dendrimers. G6 dendrimers showed greater brain accumulation and penetrating efficiency into CSF than many clinically used drugs, with CSF/serum ratios ranging between 0.02-0.2 throughout the experiment's duration. The G6 dendrimer's ability to penetrate the blood brain barrier was associated with the severity of inflammation, with higher dendrimer accumulation in the injured brain from animals having higher CSF levels of pro-inflammatory cytokines. Our results also suggest that G6 dendrimers specifically target microglia and injured neuronal cells, the major cell types associated with neuroinflammation and excitotoxicity. This suggests G6 dendrimers may be powerful vehicles to deliver potent drugs that attenuate these two major injury mechanisms. The

relatively high dendrimer levels in the CNS may be attributed to an extended systemic circulation due to the size of G6 dendrimers, which lie in the intermediate range for glomerular filtration (6.7 nm). Dendrimers of such size avoid rapid renal or RES clearance as compared to smaller dendrimers, but are still small enough to penetrate an impaired BBB. This clinically relevant large animal model provides a conceptual framework for how dendrimer-based drug delivery systems may potentiate existing therapies and merits consideration as a translational model for future trials involving CNS pharmacotherapies.

Supplementary Material

Refer to Web version on PubMed Central for supplementary material.

Acknowledgements

This work was supported by National Institutes of Health (R01 HL091541-21 [WAB], 2015, R01 EB018306 [RMK], R01 HD076901 [RMK]). The authors would like to acknowledge Melissa Jones and Jeffery Brawn for their help with animal care and surgical procedures, and Nufar Chaban for her help in tissue cryosection. The authors would also like to thank Wilmer Eye Institute core facility for the access to LSM 710 confocal microscopy.

References

1. Bigelow WG, Callaghan JC, Hopps JA. General hypothermia for experimental intracardiac surgery; the use of electrophrenic respirations, an artificial pacemaker for cardiac standstill and radio-frequency rewarming in general hypothermia. Ann Surg. 1950; 132:531–539. [PubMed: 15433219]
2. Bigelow WG, Mcbirnie JE. Further Experiences with Hypothermia for Intracardiac Surgery in Monkeys and Groundhogs. Annals of Surgery. 1953; 137:361–365. [PubMed: 13031466]
3. Barnard CN, Schrire V. The surgical treatment of acquired aneurysm of the throracic aorta. Thorax. 1963; 18:101–115. [PubMed: 13966731]
4. Gill PS, Harrington W Jr. Kaplan MH, Ribeiro RC, Bennett JM, Liebman HA, Bernstein-Singer M, Espina BM, Cabral L, Allen S, et al. Treatment of adult T-cell leukemia-lymphoma with a combination of interferon alfa and zidovudine. N Engl J Med. 1995; 332:1744–1748. [PubMed: 7760890]
5. Svensson LG, Crawford ES, Hess KR, Coselli JS, Raskin S, Shenaq SA, Safi HJ. Deep hypothermia with circulatory arrest. Determinants of stroke and early mortality in 656 patients. J Thorac Cardiovasc Surg. 1993; 106:19–28. discussion 28-31. [PubMed: 8321002]
6. Redmond JM, Gillinov AM, Zehr KJ, Blue ME, Troncoso JC, Reitz BA, Cameron DE, Johnston MV, Baumgartner WA. Glutamate excitotoxicity: a mechanism of neurologic injury associated with hypothermic circulatory arrest. J Thorac Cardiovasc Surg. 1994; 107:776–786. discussion 786-777. [PubMed: 8127107]
7. Tseng EE, Brock MV, Lange MS, Troncoso JC, Blue ME, Lowenstein CJ, Johnston MV, Baumgartner WA. Glutamate excitotoxicity mediates neuronal apoptosis after hypothermic circulatory arrest. Ann Thorac Surg. 2010; 89:440–445. [PubMed: 20103318]
8. van Harten AE, Scheeren TW, Absalom AR. A review of postoperative cognitive dysfunction and neuroinflammation associated with cardiac surgery and anaesthesia. Anaesthesia. 2012; 67:280–293. [PubMed: 22321085]
9. Blue ME, Wilson MA, Beaty CA, George TJ, Arnaoutakis GJ, Haggerty KA, Jones M, Brawn J, Manmohan S, Lange MS, Johnston MV, Baumgartner WA, Troncoso JC. Brain injury in canine models of cardiac surgery. J Neuropathol Exp Neurol. 2014; 73:1134–1143. [PubMed: 25383634]
10. Barreiro CJ, Williams JA, Fitton TP, Lange MS, Blue ME, Kratz L, Barker PB, Degaonkar M, Gott VL, Troncoso JC, Johnston MV, Baumgartner WA. Noninvasive assessment of brain injury in a canine model of hypothermic circulatory arrest using magnetic resonance spectroscopy. Annals of Thoracic Surgery. 2006; 81:1593–1598. [PubMed: 16631640]

11. Williams JA, Barreiro CJ, Nwakanma LU, Lange MS, Kratz LE, Blue ME, Berrong J, Patel ND, Gott VL, Troncoso JC, Johnston MV, Baumgartner WA, Hammon JW, Wheatley GH, Kouchoukos NT, Kurlansky P. Valproic acid prevents brain injury in a canine model of hypothermic circulatory arrest: A promising new approach to neuroprotection during cardiac surgery. Annals of Thoracic Surgery. 2006; 81:2235–2242. [PubMed: 16731160]
12. Mishra MK, Beaty CA, Lesniak WG, Kambhampati SP, Zhang F, Wilson MA, Blue ME, Troncoso JC, Kannan S, Johnston MV, Baumgartner WA, Kannan RM. Dendrimer brain uptake and targeted therapy for brain injury in a large animal model of hypothermic circulatory arrest. ACS Nano. 2014; 8:2134–2147. [PubMed: 24499315]
13. Cornford EM, Diep CP, Pardridge WM. Blood-brain barrier transport of valproic acid. J Neurochem. 1985; 44:1541–1550. [PubMed: 3921665]
14. Kakee A, Takanaga H, Hosoya K, Sugiyama Y, Terasaki T. In vivo evidence for brain-to-blood efflux transport of valproic acid across the blood-brain barrier. Microvasc Res. 2002; 63:233–238. [PubMed: 11866547]
15. Sunitha K, Hemshekhar M, Thushara RM, Santhosh MS, Yariswamy M, Kemparaju K, Girish KS. N-Acetylcysteine amide: a derivative to fulfill the promises of N-Acetylcysteine. Free Radic Res. 2013; 47:357–367. [PubMed: 23472882]
16. Kannan S, Dai H, Navath RS, Balakrishnan B, Jyoti A, Janisse J, Romero R, Kannan RM. Dendrimer-Based Postnatal Therapy for Neuroinflammation and Cerebral Palsy in a Rabbit Model. Sci Transl Med. 2012; 4
17. Zhang F, Mastorakos P, Mishra MK, Mangraviti A, Hwang L, Zhou J, Hanes J, Brem H, Olivi A, Tyler B, Kannan RM. Uniform brain tumor distribution and tumor associated macrophage targeting of systemically administered dendrimers. Biomaterials. 2015; 52:507–516. [PubMed: 25818456]
18. Burd I, Zhang F, Dada T, Mishra MK, Borbiev T, Lesniak WG, Baghlaf H, Kannan S, Kannan RM. Fetal uptake of intra-amniotically delivered dendrimers in a mouse model of intrauterine inflammation and preterm birth. Nanomedicine. 2014; 10:1343–1351. [PubMed: 24657482]
19. Owens DE 3rd, Peppas NA. Opsonization, biodistribution, and pharmacokinetics of polymeric nanoparticles. Int J Pharm. 2006; 307:93–102. [PubMed: 16303268]
20. Yu M, Zheng J. Clearance Pathways and Tumor Targeting of Imaging Nanoparticles. ACS Nano. 2015; 9:6655–6674. [PubMed: 26149184]
21. Giri J, Diallo MS, Simpson AJ, Liu Y, Goddard WA, Kumar R, Woods GC. Interactions of poly(amidoamine) dendrimers with human serum albumin: binding constants and mechanisms. ACS Nano. 2011; 5:3456–3468. [PubMed: 21438566]
22. Blanco E, Shen H, Ferrari M. Principles of nanoparticle design for overcoming biological barriers to drug delivery. Nat Biotechnol. 2015; 33:941–951. [PubMed: 26348965]
23. Lee JH, Park G, Hong GH, Choi J, Choi HS. Design considerations for targeted optical contrast agents. Quant Imaging Med Surg. 2012; 2:266–273. [PubMed: 23289086]
24. Gibson JG, Keeley JL, Pijoan M. The Blood Volume of Normal Dogs. Am J Physiol. 1938; 121:800–806.
25. Rodrigues AM, Radominski RB, Suplicy Hde L, De Almeida SM, Niclewicz PA, Boguszewski CL. The cerebrospinal fluid/serum leptin ratio during pharmacological therapy for obesity. J Clin Endocrinol Metab. 2002; 87:1621–1626. [PubMed: 11932292]
26. Wolff T, Samuelsson H, Hedner T. Concentrations of morphine and morphine metabolites in CSF and plasma during continuous subcutaneous morphine administration in cancer pain patients. Pain. 1996; 68:209–216. [PubMed: 9121807]
27. Brzakovic B, Pokrajac M, Dzoljic E, Levic Z, Varagic VM. Cerebrospinal fluid and plasma pharmacokinetics of phenobarbital after intravenous administration to patients with status epilepticus. Clin Drug Invest. 1997; 14:307–313.
28. Nau R, Sorgel F, Eiffert H. Penetration of Drugs through the Blood-Cerebrospinal Fluid/Blood-Brain Barrier for Treatment of Central Nervous System Infections. Clin Microbiol Rev. 2010; 23:858. [PubMed: 20930076]

29. Okamura T, Ishibashi N, Kumar TS, Zurakowski D, Iwata Y, Lidov HG, Jonas RA. Hypothermic circulatory arrest increases permeability of the blood brain barrier in watershed areas. Ann Thorac Surg. 2010; 90:2001–2008. [PubMed: 21095352]
30. Bartels K, Ma Q, Venkatraman TN, Campos CR, Smith L, Cannon RE, Podgoreanu MV, Lascola CD, Miller DS, Mathew JP. Effects of deep hypothermic circulatory arrest on the blood brain barrier in a cardiopulmonary bypass model--a pilot study. Heart Lung Circ. 2014; 23:981–984. [PubMed: 24931068]
31. Johnson TA, Stasko NA, Matthews JL, Cascio WE, Holmuhamedov EL, Johnson CB, Schoenfisch MH. Reduced ischemia/reperfusion injury via glutathione-initiated nitric oxide-releasing dendrimers. Nitric Oxide. 2010; 22:30–36. [PubMed: 19914388]
32. Nance E, Porambo M, Zhang F, Mishra MK, Buelow M, Getzenberg R, Johnston M, Kannan RM, Fatemi A, Kannan S. Systemic dendrimer-drug treatment of ischemia-induced neonatal white matter injury. J Control Release. 2015; 214:112–120. [PubMed: 26184052]
33. Sarin H, Kanevsky AS, Wu HT, Brimacombe KR, Fung SH, Sousa AA, Auh S, Wilson CM, Sharma K, Aronova MA, Leapman RD, Griffiths GL, Hall MD. Effective transvascular delivery of nanoparticles across the blood-brain tumor barrier into malignant glioma cells. J Transl Med. 2008; 6
34. Curtis C, Zhang M, Liao R, Wood T, Nance E. Systems-level thinking for nanoparticle-mediated therapeutic delivery to neurological diseases. Wiley Interdiscip Rev Nanomed Nanobiotechnol. 2016
35. Redmond JM, Zehr KJ, Blue ME, Lange MS, Gillinov AM, Troncoso JC, Cameron DE, Johnston MV, Baumgartner WA. AMPA glutamate receptor antagonism reduces neurologic injury after hypothermic circulatory arrest. Ann Thorac Surg. 1995; 59:579–584. [PubMed: 7887693]
36. Dommergues MA, Plaisant F, Verney C, Gressens P. Early microglial activation following neonatal excitotoxic brain damage in mice: a potential target for neuroprotection. Neuroscience. 2003; 121:619–628. [PubMed: 14568022]
37. Grimm JC, Magruder JT, Wilson MA, Blue ME, Crawford TC, Troncoso JC, Zhang F, Kannan S, Sciortino CM, Johnston MV, Kannan RM, Baumgartner WA. Nanotechnology Approaches to Targeting Inflammation and Excitotoxicity in a Canine Model of Hypothermic Circulatory Arrest-Induced Brain Injury. Ann Thorac Surg. 2016
38. Hutter E, Boridy S, Labrecque S, Lalancette-Hebert M, Kriz J, Winnik FM, Maysinger D. Microglial response to gold nanoparticles. ACS Nano. 2010; 4:2595–2606. [PubMed: 20329742]
39. Zhang F, Lin YA, Kannan S, Kannan RM. Targeting specific cells in the brain with nanomedicines for CNS therapies. J Control Release. 2015
40. Papa S, Ferrari R, De Paola M, Rossi F, Mariani A, Caron I, Sammali E, Peviani M, Dell'Oro V, Colombo C, Morbidelli M, Forloni G, Perale G, Moscatelli D, Veglianese P. Polymeric nanoparticle system to target activated microglia/macrophages in spinal cord injury. J Control Release. 2014; 174:15–26. [PubMed: 24225226]
41. Papa S, Rossi F, Ferrari R, Mariani A, De Paola M, Caron I, Fiordaliso F, Bisighini C, Sammali E, Colombo C, Gobbi M, Canovi M, Lucchetti J, Peviani M, Morbidelli M, Forloni G, Perale G, Moscatelli D, Veglianese P. Selective nanovector mediated treatment of activated proinflammatory microglia/macrophages in spinal cord injury. ACS Nano. 2013; 7:9881–9895. [PubMed: 24138479]
42. Zhang F, Nance E, Alnasser Y, Kannan R, Kannan S. Microglial migration and interactions with dendrimer nanoparticles are altered in the presence of neuroinflammation. J Neuroinflammation. 2016; 13:65. [PubMed: 27004516]
43. Haney MJ, Klyachko NL, Zhaoa YL, Gupta R, Plotnikova EG, He ZJ, Patel T, Piroyan A, Sokolsky M, Kabanov AV, Batrakova EV. Exosomes as drug delivery vehicles for Parkinson's disease therapy. Journal of Controlled Release. 2015; 207:18–30. [PubMed: 25836593]
44. Kumar P, Wu HQ, McBride JL, Jung KE, Kim MH, Davidson BL, Lee SK, Shankar P, Manjunath N. Transvascular delivery of small interfering RNA to the central nervous system. Nature. 2007; 448:39–43. [PubMed: 17572664]
45. Vidal F, Vasquez P, Diaz C, Nova D, Alderete J, Guzman L. Mechanism of PAMAM Dendrimers Internalization in Hippocampal Neurons. Mol Pharm. 2016

46. Sadekar S, Ray A, Janat-Amsbury M, Peterson CM, Ghandehari H. Comparative biodistribution of PAMAM dendrimers and HPMA copolymers in ovarian-tumor-bearing mice. Biomacromolecules. 2011; 12:88–96. [PubMed: 21128624]

47. Zhang CL, Li C, Liu YL, Zhang JP, Bao CC, Liang SJ, Wang Q, Yang Y, Fu HL, Wang K, Cui DX. Gold Nanoclusters-Based Nanoprobes for Simultaneous Fluorescence Imaging and Targeted Photodynamic Therapy with Superior Penetration and Retention Behavior in Tumors. Adv Funct Mater. 2015; 25:1314–1325.

48. Benezra M, Penate-Medina O, Zanzonico PB, Schaer D, Ow H, Burns A, DeStanchina E, Longo V, Herz E, Iyer S, Wolchok J, Larson SM, Wiesner U, Bradbury MS. Multimodal silica nanoparticles are effective cancer-targeted probes in a model of human melanoma. J Clin Invest. 2011; 121:2768–2780. [PubMed: 21670497]

49. Alric C, Miladi I, Kryza D, Taleb J, Lux F, Bazzi R, Billotey C, Janier M, Perriat P, Roux S, Tillement O. The biodistribution of gold nanoparticles designed for renal clearance. Nanoscale. 2013; 5:5930–5939. [PubMed: 23702968]

50. Kannan RM, Nance E, Kannan S, Tomalia DA. Emerging concepts in dendrimer-based nanomedicine: from design principles to clinical applications. J Intern Med. 2014; 276:579–617. [PubMed: 24995512]

51. Zhao YF, Sultan D, Detering L, Luehmann H, Liu YJ. Facile synthesis, pharmacokinetic and systemic clearance evaluation, and positron emission tomography cancer imaging of Cu-64-Au alloy nanoclusters. Nanoscale. 2014; 6:13501–13509. [PubMed: 25266128]

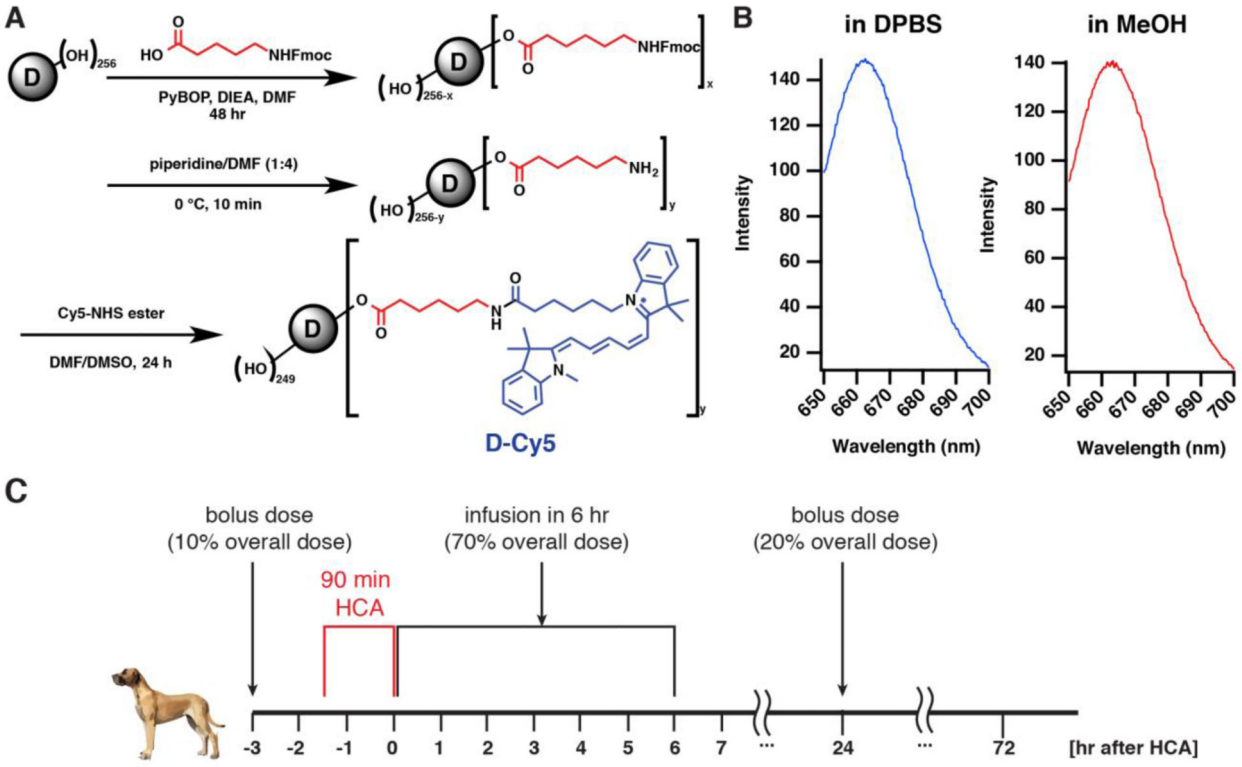

Figure 1.

(A) Synthesis route of G6-Cy5. **(B)** Fluorescence emission spectrum of G6-Cy5 in DPBS and MeOH. Excitation: 645 nm. **(C)** Experimental procedure for dendrimer administration in a canine model of post-HCA brain injury.

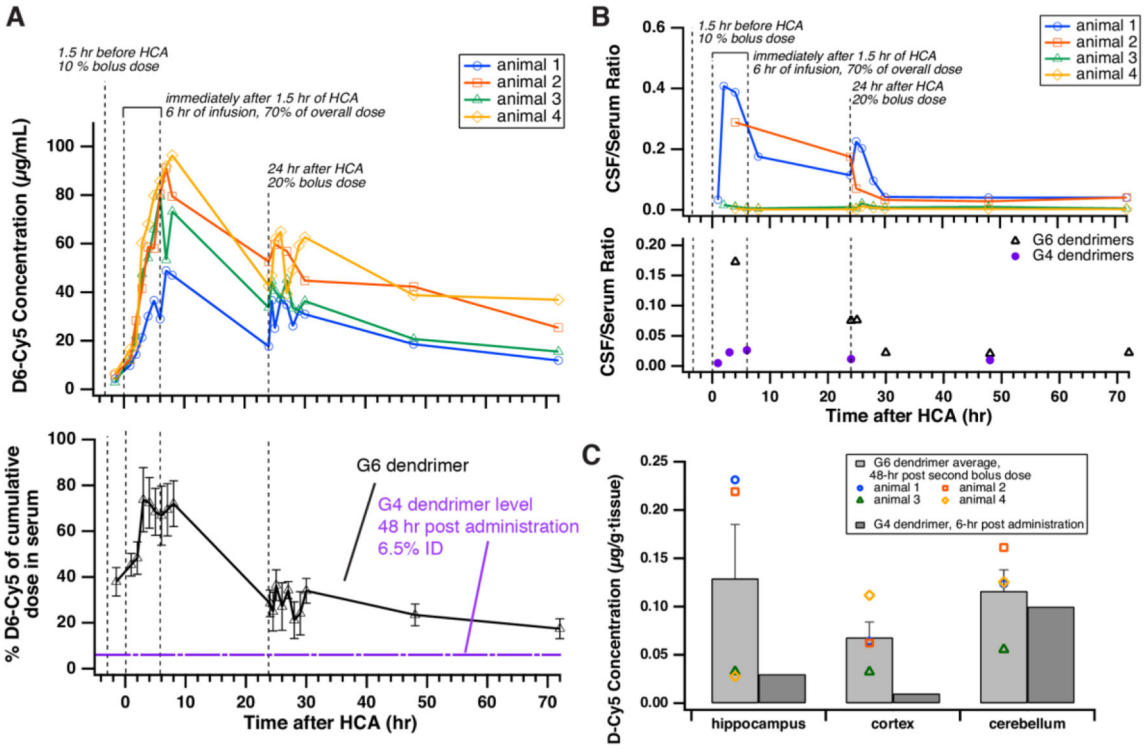

Figure 2. G6-Cy5 has prolonged serum circulation and high accumulation in the brain of HCA animals

(A) Concentration of G6-Cy5 in the serum of each animal tested over time **(top)**, and mean percent of G6-Cy5 + SEM (black solid line) compared to G4 dendrimer level at 48 hrs post administration (purple dotted line) **(bottom)**. **(B)** The CSF/Serum ratio of each animal as function of time **(top)**, and mean values (black triangles), as compared to G4 dendrimer CSF/serum ratio (purple dots) **(bottom)**. **(C)** The accumulation of G6-Cy5 within injured brain regions (hippocampus, cortex, and cerebellum) at 48 hrs after the last dose of G6-Cy5 for each animal (scatter plot) and mean values (light gray bars) versus the accumulation of G4-Cy5 (dark bars) in these regions at 6 hrs after infusion. All the data related to G4 dendrimers in this figure were adapted from published data: Mishra MK, et. al, ACS Nano. 2014 Mar 25;8(3):2134-47.

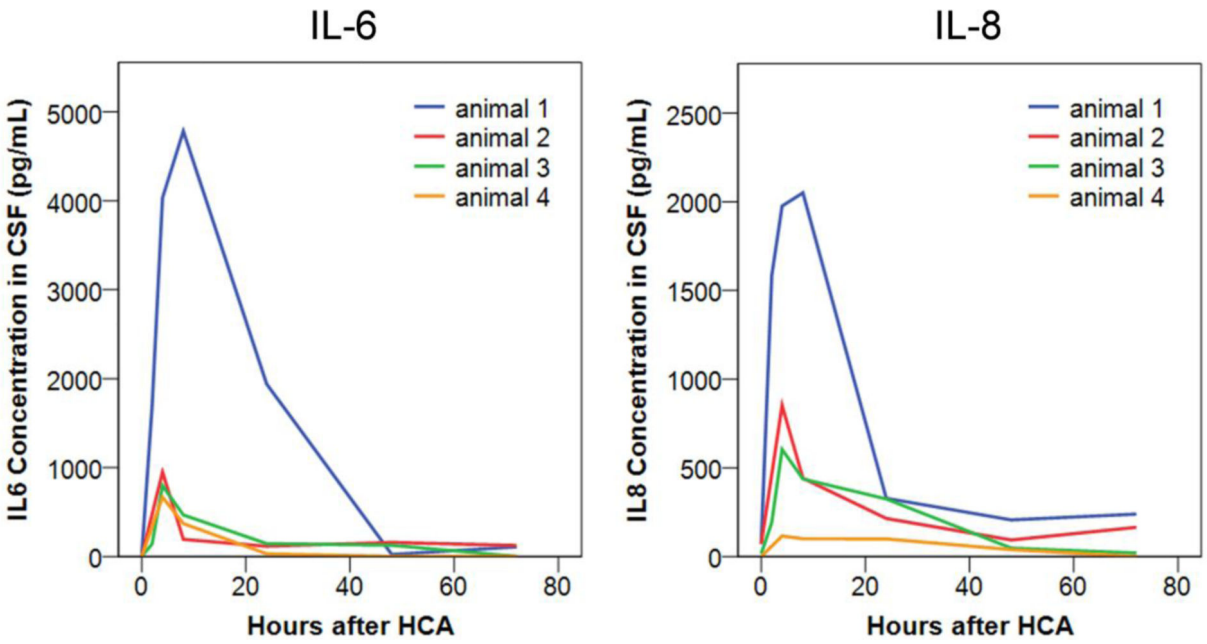

Figure 3. IL-6 (left) and IL-8 (right) concentration in the CSF of 4 animals after HCA

Cytokine levels were measured at different time points after HCA using ELISA.

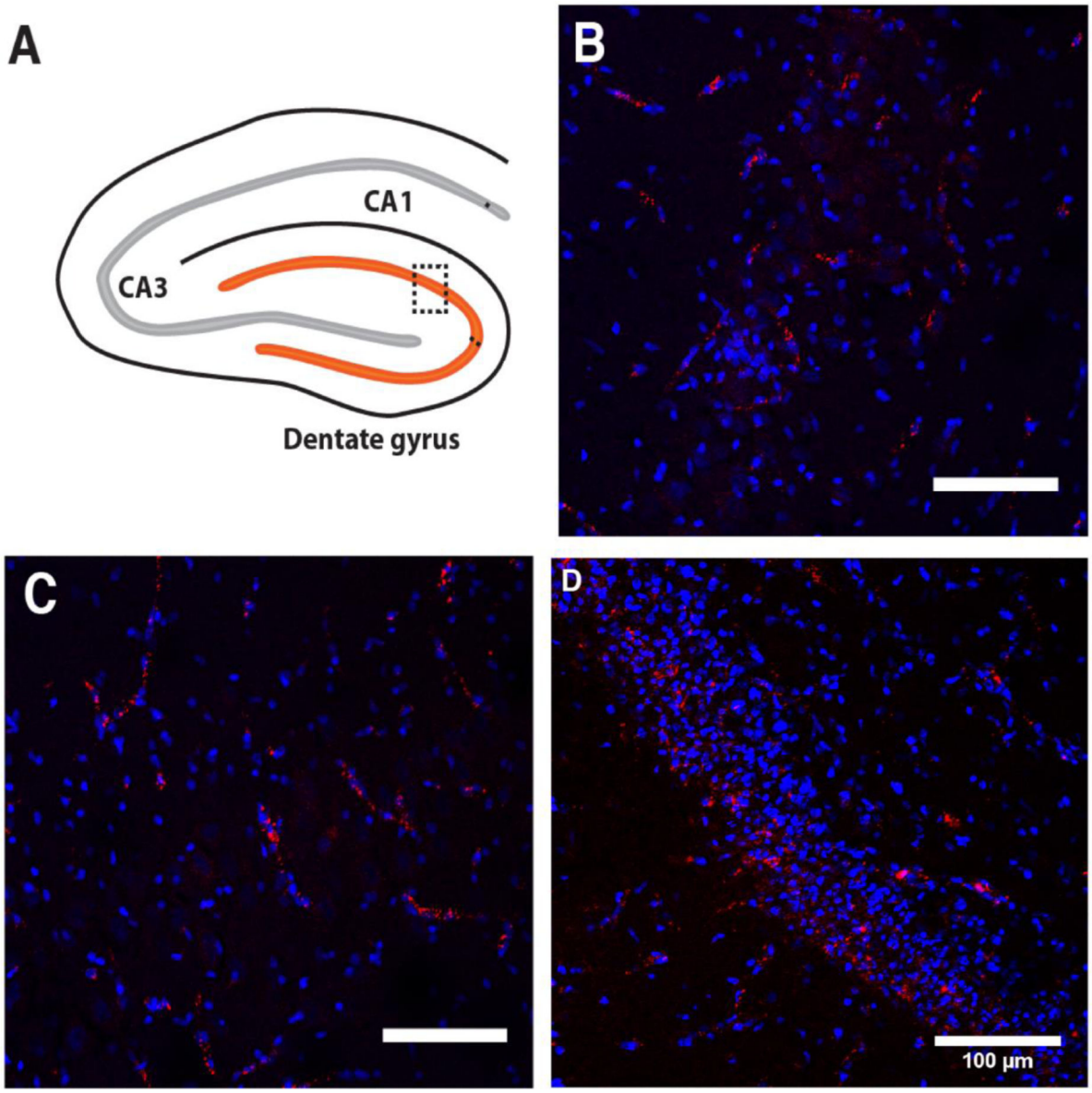

Figure 4.

(A) Schematic representation of sampling within the hippocampus, the most injured brain region after HCA in this model. **(B-D)** Confocal microscopic images of CA1 **(B)**, CA3 **(C)**, and dentate gyrus **(D)**, blue: DAPI; red: G6-Cy5. Scale bars = 100 μm.

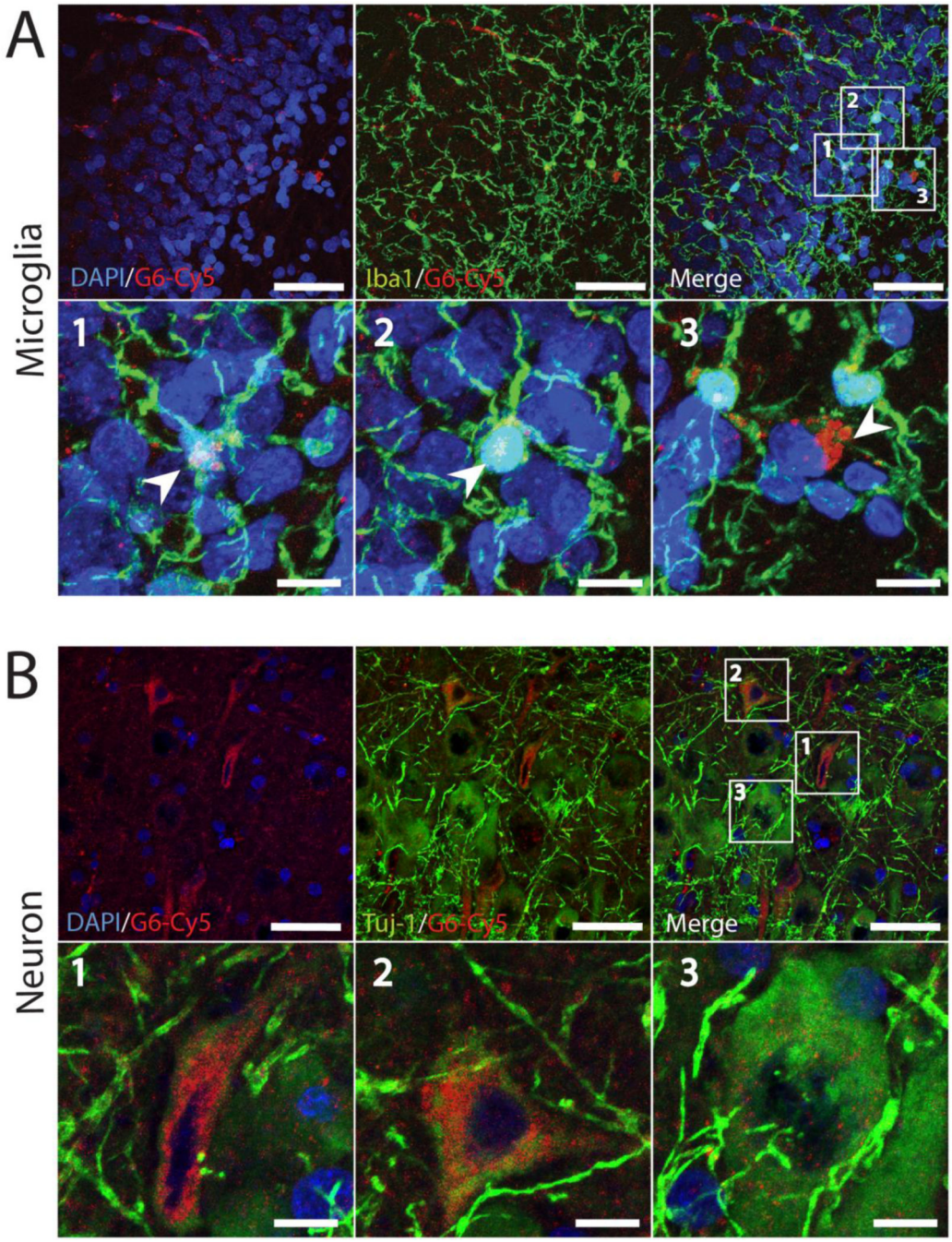

Figure 5.

The localization of G6-Cy5 within microglia/macrophages **(A)**, and neurons **(B)** in the injured hippocampus, 72 hrs after HCA. In magnified images, G6-Cy5 is localzed within Iba-1-positive microglial cells (green; arrowheads) **(A)** and TUJ1-positive neurons (green) **(B).** For all images, red: G6-Cy5 and blue: DAPI-labeled nuclei. (bars = 50 μm or 10 μm for zoomed in regions).

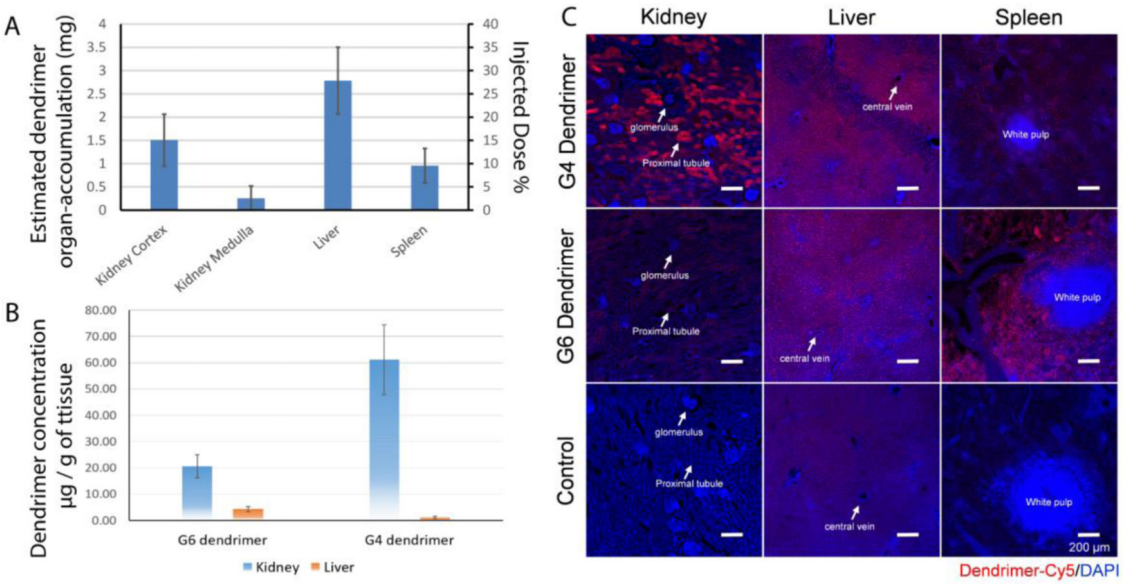

Figure 6. The biodistribution of G6 dendrimers in major organs

(A) The estimated G6-Cy5 uptake by the major organs (kidney, liver, spleen) at the end of experiment, with 180 mg as the total injected dose. **(B)** The comparison of G6 *vs.* G4 dendrimer concentration in kidney (blue) and liver (orange) at 48 hrs after the administration of last dose. All the data related to G4 dendrimers from this figure were adapted from published data: Mishra MK, et. al, ACS Nano. 2014 Mar 25;8(3):2134-47. Since most accumulated G6 dendrimer in kidney locates in the cortex, dendrimer accumulation in kidney was approximated by the averaged concentrations from the cortex and medulla. **(C)** The confocal microscope images showed G6 dendrimers distribution in the major organs (kidney, liver, spleen) after HCA. Red: G6-Cy5, Blue: DAPI-labeled nuclei. Scale: 200 µm.

Table 1

The ratio of urine AUC to serum AUC indicates the decreased renal clearance rate for G6 dendrimers, compared with G4 dendrimers.

	G6 dendrimer	G4 dendrimer
Time of HCA	1.5 hrs	2.0 hrs
Administration method	1st dose: 10% bolus dose at 3 hr before HCA conclusion; 2nd dose: 70% i.v. infusion 0-6 hrs after HCA; 3rd dose: 20% bolus dose at 24 hrs after HCA.	A single dose of 1 hr i.v. infusion after HCA
Dose	6 mg/kg	5 mg/kg
Urine AUC/ Serum AUC	0.57	3.77

Table 2

G4 and G6 dendrimer accumulation within injured brain regions and major organs in a canine model of HCA. In the G6 biodistribution study, animals underwent 1.5 hrs of HCA and dendrimers were given at a dose of 6 mg/kg (based on 30 kg animal weight, the total injection dose per animal is 180 mg). In the G4 biodistribution study, animals underwent 2.0 hrs of HCA and dendrimers were given at a dose of 5 mg/kg (based on 30 kg animal weight, the total injection dose per animal is 150 mg).

Organs	Dendrimer accumulation / gram of tissue (μg/g)		
	G6 at 48 hrs post last dose	G4 at 6 hrs post i.v.	G4 at 48 hrs post i.v.
Brain hippocampus	0.13	0.03	Below detection
Brain cerebellum	0.12	0.06	Below detection
Brain cortex	0.11	0.01	Below detection
Kidney	20.70	99.43	61.20
Liver	4.63	3.78	1.12
Heart	0.76	0.28	1.25
Lung	0.83	0.98	2.20
Pancreas	0.11	1.75	0.90